

Towards the understanding of Keim'sche Mineralfarben in architectural paints: Material characterization and phase quantification on selected historical pigment admixtures

Yee Wu^{a,b} , Eva Mariasole Angelin^b , Thomas Danzl^b , SoHyun Park^a , Clarimma Sessa^{b,*} 

^a Department of Geo- and Environmental Sciences, Section of Crystallography, Ludwig-Maximilians-Universität München (LMU), Theresienstr. 41C, 80333, Munich, Germany

^b Chair of Conservation-Restoration, Art Technology and Conservation Science, Technical University of Munich, Oettingenstr. 15, 80538, Munich, Germany

ARTICLE INFO

Keywords:

Keim'sche mineralfarben
Silicate paint
Architectural surfaces
Historical pigments
Non-destructive methods
Rietveld refinement

ABSTRACT

'Keim'sche Mineralfarben' are widely recognized silicate-based paints historically employed for painting and decorating architectural surfaces, as well as in the conservation and restoration of historic buildings and monuments, particularly where high-quality architectural finishes are required. Comprehensive knowledge of the composition of historical Keim'sche Mineralfarben pigment admixtures and their evolution—particularly for dating purposes—remains limited within the field of architectural conservation. The study demonstrates the effectiveness of a multi-analytical approach in characterizing the composition and phase quantification of selected yellow-to brownish-toned historical Keimfarben pigment admixtures and suggests a methodology for the characterization of this product on site, offering new perspectives on understanding the chronology of the paint layers, thus planning future restoration interventions. A multi-analytical approach was employed, combining optical microscopy, X-ray fluorescence, in situ Raman and micro-Raman spectroscopy, ATR-FTIR, and X-ray powder diffraction with Rietveld refinement. The results show that the studied Keimfarben pigment admixtures are composed of calcite, fluorite, kaolinite, quartz, barite, rutile, and witherite, as well as different quantities of hematite, goethite, and eskolaite depending on the hue. Certain identified phases have been shown to serve as diagnostic markers, limiting the application of the examined products on architectural surfaces to the period between the 1958 and 1980s. Moreover, quantitative analysis of the components may help elucidate their function within the admixture and will be essential for advancing the investigation into their relevance in the coating's formation.

1. Introduction

Keim'sche Mineralfarben developed by Adolf Wilhelm Keim and patented in 1878, are renowned for their exceptional durability, weather resistance, and aesthetic performance [1]. These qualities have established them as a preferred choice not only in the fields of fine art, architecture, and decorative painting but also in the conservation and restoration of historic buildings [1]. This invention was driven by the need for new façade painting techniques as well as stable products for reconstruction and conservation-restoration intervention, as existing wall paintings in the open air faced significant durability issues. Keimfarben therefore emerged as a inorganic solution for architecture [2].

Based on a mineral binder system—primarily potassium silicate

(water glass)—these paints form a strong, insoluble chemical bond with mineral substrates through a process known as silicification. This results in highly stable, breathable coatings that distinguish them from conventional film-forming paints [3].

Since the first patent and the founding of today's company, KEIM-FARBEN GmbH, the fundamental formulation of its silicate paint systems has remained largely unchanged. This is consistently emphasized by the company, reflecting its commitment to product quality and performance, and/or possibly due to the limitations of compounds suitable for forming a stable silicate-based paint system [4,5].

The precise formulations of Keim products still remain proprietary, presenting significant challenges for researchers and conservators attempting to distinguish between historical paint layers and subsequent

* Corresponding author.

E-mail address: clarimma.sessa@tum.de (C. Sessa).

<https://doi.org/10.1016/j.dyepig.2025.113285>

Received 11 July 2025; Received in revised form 24 September 2025; Accepted 25 September 2025

Available online 26 September 2025

0143-7208/© 2025 The Authors. Published by Elsevier Ltd. This is an open access article under the CC BY license (<http://creativecommons.org/licenses/by/4.0/>).

restoration interventions, especially within the framework of the two-component system (consisting of a pigment powder and a liquid fixative). This difficulty is particularly evident in the conservation of historical buildings, where successive applications of similar or identical silicate products may obscure the stratigraphic differentiation between historical and later-applied layers.

To date, the only conference specifically dedicated to the understanding of Keimfarben and their implications for conservation practice—was held in 1997 at the ETH Zurich under the title "*Erfahrungen mit der Restaurierung von Mineralfarbenmalereien*". Organized by the Institute for Monument Preservation, the event brought together experts from restoration, materials science, and architectural history to discuss the history, materiality, and conservation challenges of mineral-based wall paintings and façade finishes. The proceedings, published under the title "*Mineralfarben: Beiträge zur Geschichte und Restaurierung von Fassadenmalereien und Anstrichen*", remain the only comprehensive publication to date focusing on the practical and theoretical aspects of Keim's silicate paint systems. This milestone conference marked the first and, so far, only systematic attempt to consolidate historical, technical, and conservation knowledge about these materials that is essential for informed restoration approaches [1]. The doctoral thesis of Osswald, which summary is also present in the publication of the conference, offers valuable insights into curing mechanisms in silicate paints, particularly regarding cation-induced gel formation. However, it was not able to fully disclose the complexity of historical Keimfarben formulations and understanding the factors of their stability [6]. A comprehensive study has been published by Alp et al., re-opens the discussion of the identification and discrimination of Keim paint from other brands products focusing on the early production between 1920 and 1930 [7].

The present study represents a further step toward understanding the chronological evolution of Keimfarben production by investigating a selection of historical Keim products donated to the Chair of Conservation-Restoration at the Technical University of Munich (TUM). The analyzed materials was owned by the painting company (*Malergeschäft*) *Edmund Kölbel*, founded in 1927 in Lindau, Germany, which operated across two generations. After the Company was taken over by the son of the founder (1962), it specialized in the use of mineral-based paints, particularly Keim products. Among the most notable projects was the restoration of the façade of the *Lindau Rathaus* (Town Hall) [8] carried out by the conservator Josef Lorch (1929–1999) in collaboration with the founder's son and the local monument care office between 1972 and 1974 [9].

The preserved material stock—including dry pigments and prepared mixtures—offers a valuable insight into materials used in the historical areas of Lindau from the 1960s through the early 2000s. Though not systematically documented, the collection reflects authentic, practice-based knowledge of silicate paint application in heritage contexts [10].

The aim of this study is twofold: (1) to carry out an exhaustive material characterization and phase quantification of a selection of historical Keim products using a multi-analytical approach; and (2) to evaluate the potential for identifying such materials in situ within architectural stratigraphies, particularly for dating interventions or distinguishing between historical applications from later restoration intervention/repainting campaigns. Since the donation comprised 188 different Keimfarben products, a selection was necessary. The chosen set does not encompass the entire historical Keimfarben pigment palette but constitutes a representative specific chromatic subset ranging from yellow to brown hues, allowing for an in-depth material characterization while maintaining a manageable analytical scope.

An underlying question addressed in this study concerns the role of individual components and their proportion, such as pigments and fillers, within the broader paint system. Particular emphasis is placed on reviewing literature about which interactions among these constituents are critical for the curing mechanisms and how they influence the long-term stability and performance of the material.

The multi-analytical approach employed in this study combines non-invasive and micro-invasive techniques, including portable X-ray fluorescence (XRF) and Raman spectroscopies, with laboratory-based analyses such as ATR-FTIR spectroscopy, micro-Raman spectroscopy, and X-ray diffraction (XRD) with Rietveld refinement for quantitative phase analysis. This combined approach permitted to balance the need for non-destructive, in situ-compatible analysis using portable instrumentation with the enhanced capabilities of advanced laboratory techniques. By comparing qualitative and quantitative results from both settings, the study also permitted to assess the potential and limitations of portable methods—particularly regarding their detection limits and reliability for in situ applications. These findings are especially relevant for heritage conservation contexts, where minimally invasive strategies are essential, and decision-making often relies on rapid yet accurate material identification directly on-site.

1.1. Keim Farben paint system

A Keim mineral paint system is defined as a mineral-based coating in which a potassium silicate (water glass) binder chemically reacts with mineral substrates. Historically, two main paint systems have been recognized for Keimfarben: the traditional two-component system, consisting of a liquid potassium silicate ("*Fixative*") and a mineral pigment admixture ("*Farbpulver*"), and the one-component system, in which all ingredients are combined in a single product. According to German standard DIN 18363, Section 2.4.1, no organic constituents are present in two-component formulations. The first one-component system, known as *Dispersionssilikatfarben*, was introduced in the 1960s. It is composed of potassium silicate, pigment admixtures, and a small proportion of organic components. Since the 2000s, modified variants containing silica sol, known as *Kieselsolefarben* (potassium silicate/silica sol/pigment admixtures/organic substances), have also become available. In general, the organic content in one-component systems is less than 5 % [11]. The presence of organic constituents in the one-component system is also the key distinction between the two systems.

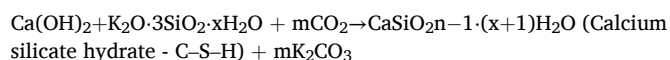
The chemical processes involved in the hardening of silicate paints on the substrate involve the reaction of potassium water glass with mineral pigment admixture and with reactive components of the substrate. The performance of silicate coatings depends strongly on the substrate. Fresh concrete, lime, and cement plasters can cause premature coagulation of potassium silicate and must be fully carbonated and dry. Porous materials like sand-lime bricks offer good adhesion, while substrates such as gypsum, wood, glass, and metals require special pretreatment or are unsuitable due to poor chemical compatibility or mechanical stability. Proper surface preparation is essential for long-term coating performance.

Based on the literature [6,8–10], the setting of a two-component silicate paint occurs thanks to multiple reactions.

- (1) reaction of potassium silicate with atmospheric CO₂, forming silica gel (SiO₂·nH₂O) as the main binding matrix and K₂CO₃ as a by-product that can be washed away by rain or neutralized in further reactions;



- (2) reaction with Ca(OH)₂ from mineral substrates (e.g., in lime plasters or cementitious surfaces), forming C–S–H, a stable, water-insoluble compound that contributes to the hardness and durability of the paint;



and.

- (3) condensation and hardening of the silica gel as water evaporates. As the water from the applied paint evaporates, the silica gel undergoes condensation, leading to further solidification and strengthening of the paint layer. The result is a cohesive and durable mineral coating characterized by high weather resistance (non-film-forming, no peeling), excellent water vapor permeability (enabling substrate breathability), and long-term UV and color stability ensured by inorganic pigments [11].

Physical processes such as adhesion, adsorption, and mechanical interlocking also contribute to the bond between the substrate and the silicate paint layer [8].

The A–B–C technique refers to three distinct application methods for the use of the two-component mineral paint system [12]. These methods differ in the sequence and manner in which the dry pigment admixture and the liquid fixative are applied:

A-Technik - Keim-kiinstlerfarben (A Technique, Keim artistic colours): The pigment is applied to the substrate first, followed by the fixative, which is brushed or sprayed onto the surface to bond and fix the pigment into the surface.

B-Technik - Keim-Dekorfarben (B Technique, Keim decoration colours): Pigment and fixative are mixed together before application, producing a paint that is applied as a single solution.

C-Technik - Keim Purkristall/Anstrich Farben (C Technique, Keim Façade colours): The application followed the B technique, using coarser pigments and fillers ("groberer"), making the paint suitable also for facade applications.

Each technique offers different aesthetic effects and technical advantages depending on the substrate condition, desired color intensity, and working method [12].

2. Materials and methods

2.1. Keimfarben pigment admixtures

The historical collection comprises 188 pigment admixture packages associated with four distinct product categories, identified based on their original packaging labels (Fig. 1). By observing the original packaging, one can infer that all Keim Farben products were produced in the company location Industrierwerke Lohwald, which was active from 1919 until 1978 [13], giving a first temporal frame of their datation.

From the collection, twelve samples were selected to represent the overall chromatic variability observed across the four categories, with particular emphasis on yellow to brownish tones. These hues are among the most frequently employed for façades in Lindau and respect the limitations of colours permitted by the city [14] and are therefore especially relevant for heritage conservation in this context.

Strong red and blue tones were deliberately excluded from the selection based on oral testimony from the former owner of the collection, who reported that, according to local practice at the time, the use of such saturated colours on private houses was discouraged, and owners who applied them risked receiving penalties from the municipal authorities [10].

The acronyms used in this paper are presented in Table 1. Specifically, *Anstrich Farben* (AF) and *Keim Mineral Farben* (KMF) categories comprises 6 and 39 samples, respectively. For each of those categories two samples were selected. *Keimfarben* (KF) includes 39 specimens and three samples were selected instead. The original packings provide key information about the product such as the color number (or "*Farben no.*") which refers to the coloring coding used by the Keimfarben to identify their products.




Fig. 1. Images of specimens representative of the four product categories. (a) *Anstrich Farben* (AF), (b) *Keim Mineral Farbe* (KMF), (c) *Keimfarben* (KF), (d) *Keim Farbpulver* (FP).

Table 1

List of the samples selected for this study. It includes the names and numbers printed on the packages as well the acronyms used in this paper. An image of the selected samples with a color bar is presented in [Figure A.1](#).

Category	Acronym	Product Number	Sample Name	Visible image
Anstrich Farben	AF	42	AF42	
		138	AF138	
Keim Mineral Farben	KMF	138	KMF138	
		969	KMF969	
Keim Farben	KF	406	KF406	
		444	KF444	
		446	KF446	
		956	KF956	
		969	KF969	
Keim Mineral Farbe – Farbpulver	FP	366	FP366	
		452	FP452	

Table 1 (continued)

Category	Acronym	Product Number	Sample Name	Visible image
		FP53H50	FP53H50	

2.2. Analytical methods

2.2.1. Optical microscope (OM)

Samples were observed under optical microscopy using a Leica LMDM at a magnification of 10 \times . Dark field (DF) and UV ($\lambda_{\text{exc}} = 300\text{--}400\text{ nm}$) microscopic images were captured with a Leica K3C camera operated with the software Leica Application Suite X 5.5 (Leica). Live Image Builder Z option was used to capture and stack images from multiple focal planes. A small amount of pigment powder was placed onto a glass slide for microscopic observation.

2.2.2. X-ray fluorescence (XRF)

XRF measurements were performed by means of an ELIO portable energy-dispersive X-ray fluorescence spectrometer (Bruker Nano GmbH, Berlin, Germany) with a Rh-target microfocus 10–50 kV X-ray tube excitation and a 17 mm² Semiconductor Drift Detector (SDD) with CUBE technology detection. The spot measurements were performed at a 50 kV tube voltage, 80 μA tube current for 180-s live times, and a spatial resolution of approximately 1 mm. No He and no filters were used for the measurements. The detection limit is $Z < 13$ (Al) due to the working conditions in air. Calibration with an AgCu standard ensured data alignment. The data were collected and processed with ELIO 1.6.0.66 from Bruker. A small amount of pigment powder was deposited on a plastic plate. Measurements were repeated three times at different locations. Semi-quantitative data evaluation was performed with ArtTAX-Ctrl software (Intax). The signal intensities of a selected energy line for each element were normalized with respect to the Rh Rayleigh peak ($K_{\alpha 1}$ emission line at 20.216 keV).

The line selected and integrated are Ca ($K_{\alpha 1}$ 3.691); Fe_K ($K_{\alpha 1}$ 6.403); Zn_K ($K_{\alpha 1}$ 8.638) and Cr_K ($K_{\alpha 1}$ 5.414). The $K_{\alpha 1}$ line of the Ti at 4.510 overlaps with the $L_{\alpha 1}$ of the Ba so the contribution of both elements is to be considered.

2.2.3. Attenuated total reflectance fourier transform infrared (ATR-FTIR)

A portable Alpha II spectrometer (Bruker Nano GmbH, Berlin, Germany) equipped with a CenterGlow™ source, a RockSolid™ interferometer (with gold mirrors), and a temperature-controlled DTGS detector was used to acquire the infrared spectra. Measurements were performed using a dedicated ATR module (diamond crystal, single bounce). The infrared spectra were collected in the spectral range of 4000–400 cm^{-1} with 64 co-added scans for background and sample, and a spectral resolution of 4 cm^{-1} . The diamond-sampling window was cleaned with isopropanol (Sigma-Aldrich, St. Louis, MO, USA) before and after each measurement. A small amount of pigment powder was placed directly onto the diamond crystal plate, which was then pressed using a high-pressure clamp for optimal contact. Measurements were also repeated twice for all samples.

2.2.4. Raman spectroscopy

Raman spectra were acquired with a portable B&W Tek i-Raman® Plus spectrometer (Metrohm Group, Herisau, Switzerland) equipped with a high-sensitivity TE-cooled CCD detector. The spectrometer is coupled with a 785 nm excitation laser with a maximum power of 455 mW at the laser port, adjustable by the operator. The measurements were performed using a spectral range from 65 to 3350 cm^{-1} with a resolution of less than 4.5 cm^{-1} at 912 nm. The laser power was kept at

low as possible in the range of 1–20 % of the maximum output for each measurement area to avoid any laser-induced modification. The calibration of the instrument was checked using a polystyrene standard provided by the manufacturer. Both excitation and collection signals were guided by optical fibers, and a microscope objective (20× lens magnification) was used to carry out the measurements. The integrated camera of the Raman microscope allowed for the precise selection of the analysis spot, which is approximately 1 mm in diameter. Three to six different measurement points were made for each sample.

2.2.5. X-ray powder diffraction (XRD)

X-ray powder diffraction (XRD) data were collected on a X-ray powder diffractometer (XRD3003TT, GE) at 40 keV and 40 mA in the Debye-Scherrer geometry using a monochromatized X-ray, $\text{MoK}\alpha_1$ ($\lambda = 0.7093$ Å; Ge(111) monochromator). All XRD data were collected at room temperature in a range of 5° – 75° (2θ) with a step size of 0.013° for 200 s per step. The XRD data acquisition was repeated 10 times for each sample and added up for a high counting statistic. For conducting XRD, each sample was homogeneously pestled using a set of agate mortar and pestle. The powdered sample filled within a glass capillary of 0.5 mm in diameter was mounted on a goniometer. The sample capillary was centered against the X-ray beam and rotating during the data acquisition for a better statistic. Phase identification was done using the software Match [15] interface with the abank COD [16,17].

2.2.6. Rietveld analysis

The contribution of each phase to the XRD pattern directly reflects its amount in the sample because its intensity is directly proportional to the square of the so-called structure factor F_{hkl} characterized by atomic X-ray scattering powders and atomic positions, i.e., the relative intensity distribution of each phase in one XRD pattern is the fingerprint of its structure. The Rietveld refinement method [18] was employed to analyze weight ratios of all compounds present in each sample using XRD data. These quantitative phase analyses were performed by the Rietveld method with a program package, TOPAS Academic V7 [19]. After phase identification retrieved from the ICSD database [20], the starting model of each phase was taken from various sources of crystallographic information files (.cif) reported (Supplementary: Table A.1-A.11). When the correct starting model is available, this method allows for the quantification of each phase amount in the sample. All atomic structures of the phases present in our samples are well-known, and hence their atomic coordinates were fixed in the Rietveld refinements while refining their profile parameters inclusive the lattice metrics, the zero point in $2\theta^\circ$, the sample displacement, the background correction using a 10-order polynomial (Chebyshev), the peak shape using the Pseudo-Voigt function, and the peak asymmetry correction using a specific axial divergence correction function in the generic convolution of the program package:

$$F_n(\varepsilon) = \left(\frac{1}{\varepsilon_m}\right) \left(1 - \sqrt{\frac{\varepsilon_m}{\varepsilon}}\right)$$

$$\text{for } \varepsilon = 0 \text{ to } \varepsilon_m = -\left(\frac{90}{\pi}\right) \left(\frac{SL}{R_S}\right) \cot(2\theta_k)$$

, where $\varepsilon = 2\theta - 2\theta_k$, 2θ is the measured angle and $2\theta_k$ is the Bragg angle. R_S correspond to the secondary radius of the diffractometer. ε_m is in $^\circ 2\theta$. SL refer to receiving slit length in the axial plane.

The final calculated XRD pattern are compared to that observed, where their discrepancy values are given by the agreement parameters, e.g. the weighted profile residual R_{wp} and goodness-of-fit (GOF), mathematically defined [18] as follows:

$$R_{wp} = \sqrt{\frac{\sum w_i (Y_{o,i} - Y_{c,i})^2}{\sum w_{mi} Y_{o,i}^2}}$$

$$\text{GOF} = \frac{R_{wp}}{R_{exp}} = \sqrt{\frac{\sum i (Y_{o,i} - i)^2}{M - P}}$$

$$R_{exp} = \sqrt{\frac{M - P}{\sum w_i Y_{o,i}^2}}$$

, where $Y_{o,i}$ and $Y_{c,i}$ are the observed and calculated intensities at the i -th data points, respectively. M is the number of total measured points, and P is the number of parameters to be refined. The weighting $w_i \propto 1/\sigma_i^2$ with the spread σ_i .

3. Results

The samples were analyzed by means of complementary analytical methods. The multi-analytical approach comprises OM to identify possible different aggregates and their color, XRF to characterize the elemental composition, ATR-FTIR and Raman spectroscopy to determine the chemical composition of the admixtures, and lastly XRD coupled with Rietveld analysis to identify and quantify the mineralogical phases.

3.1. Optical observations

Fig. 2 shows the samples observed under dark-field microscopy. Particle sizes range from less than 1 μm to larger than 70 μm . The images reveal that the samples are composed mainly of strongly colored fine grains (<1 μm) in shades of red, brown, orange, yellow, green; white grains of both fine and coarse sizes (10–40 μm); and translucent crystals spanning fine, coarse and very coarse (>40 μm). Particle shapes are highly irregular, and the wide variability in size renders all samples markedly heterogeneous. Interestingly, under UV excitation (300–400 nm), all samples exhibit a yellowish-green luminescence (Fig. A2), which can tentatively be attributed to a common phase present in all pigment admixtures.

3.2. Chemical and mineralogical characterization

In situ non-destructive spectroscopic methods were combined with XRD and Rietveld refinement in order to characterize the chemical and mineralogical composition of the samples. Since the integration of the information obtained from the various analytical methods follows a sequential approach—i) XRF, ii) ATR-FTIR, iii) Raman, iv) XRD—the results are discussed individually for each method in the same order.

3.2.1. XRF

Fig. 3 depicts a semi-quantitative evaluation of the elements detected. In order of signal intensity, elements such as iron (Fe), calcium (Ca), zinc (Zn) and barium (Ba) were identified in all twelve samples. While chromium (Cr) was detected only in sample FP53H50. Due to the overlap of the titanium (Ti) K_α and K_β emission lines with the L_α and L_β lines of barium (Ba), the presence of Ti can not be confirmed. The $K_{\alpha 1}$ and $K_{\alpha 2}$ energy lines at 32.193 and 31.817, respectively, allow for the confirmation of the presence of barium. Differences in the relative intensities hints variations of concentration of the components of the samples. However, the higher counts variability is observed for the iron signal.

3.2.2. ATR-FTIR

Results of the ATR-FTIR analysis are displayed in Fig. 4. All spectra are mainly showing the signals of calcite (CaCO_3), kaolinite ($\text{Al}_2\text{Si}_2\text{O}_5(\text{OH})_4$), and hematite ($\alpha\text{-Fe}_2\text{O}_3$). Calcite emerges as the dominant phase in all samples. Its presence is confirmed by three characteristic carbonate-related vibrational modes: the ν_3 (asymmetric stretch) band at 1413 cm^{-1} , the ν_2 (out-of-plane bending) band at 874 cm^{-1} , and

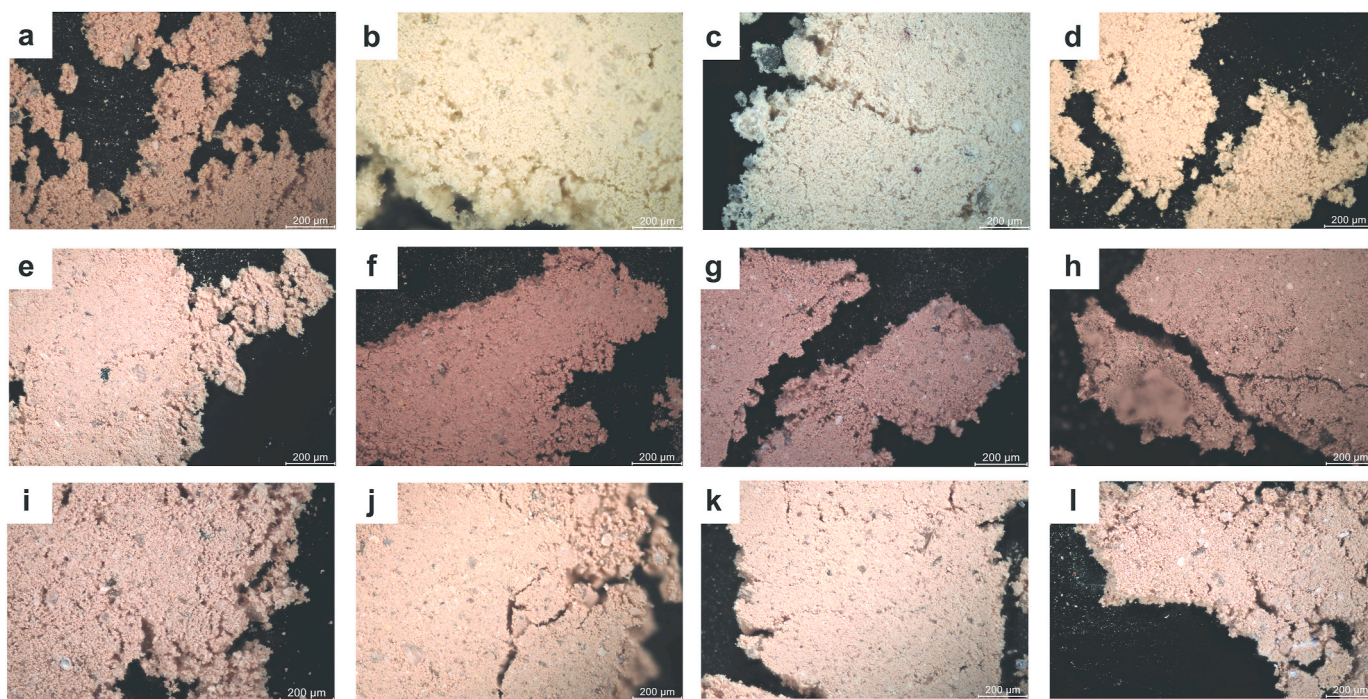


Fig. 2. Dark field microscopic images selected samples: (a) AF138 (b) AF42 (c) FP452 (d) FP366 (e) KMF138 (f) KMF969 (g) KF969 (h) FP53H50 (i) KF406 (j) KF444 (k) KF446 (l) KF956.

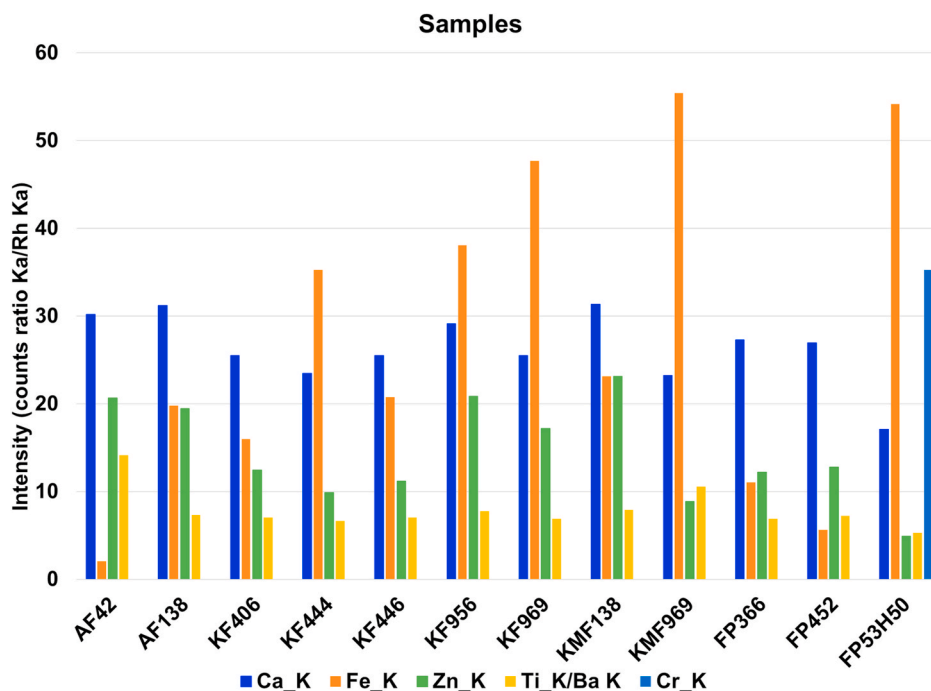


Fig. 3. Histogram of the total counts calculated for selected characteristic lines of each element, normalized to the Rh Rayleigh peak ($K_{\alpha 1}$ emission line at 20.216 keV). All the intensities reported are a mean value of three measurements.

the ν_4 (in-plane bending) band at 711 cm^{-1} [21].

The signals of kaolinite are distinguished by O–H stretching bands at 3689 and 3616 cm^{-1} , an asymmetric Si–O–Si stretching band at 1001 cm^{-1} , and Si–O stretching bands at 913 cm^{-1} [22]. Absorption peaks at 694 and 795 cm^{-1} are attributed to Si–O–Al vibrations [22]. Peak at 465 cm^{-1} suggest the presence of Fe–O vibrations [23] and the band at 531 cm^{-1} is characteristic for $\alpha\text{-Fe}_2\text{O}_3$ phase (hematite) [24].

Goethite ($\alpha\text{-FeOOH}$) is typically characterized by a distinct and

strong Fe–O vibrational band at ca. 875 cm^{-1} [25]. The different relative intensities observed in samples AF42, AF138, KF406, KF969, KMF138, FP366 and FP452 between the bands at 711 and 874 cm^{-1} of calcite can suggest the occurrence of goethite. Barite (BaSO_4) is identified in all specimens besides AF42. Barium sulfate is characterized by sulfur-oxygen (S–O) stretching vibrations in the region of $1179\text{--}1083\text{ cm}^{-1}$, with symmetrical SO_2^{4-} vibrations at 1082 cm^{-1} and out-of-plane bending vibrations at 608 and 637 cm^{-1} [26]. Infrared spectra of the AF

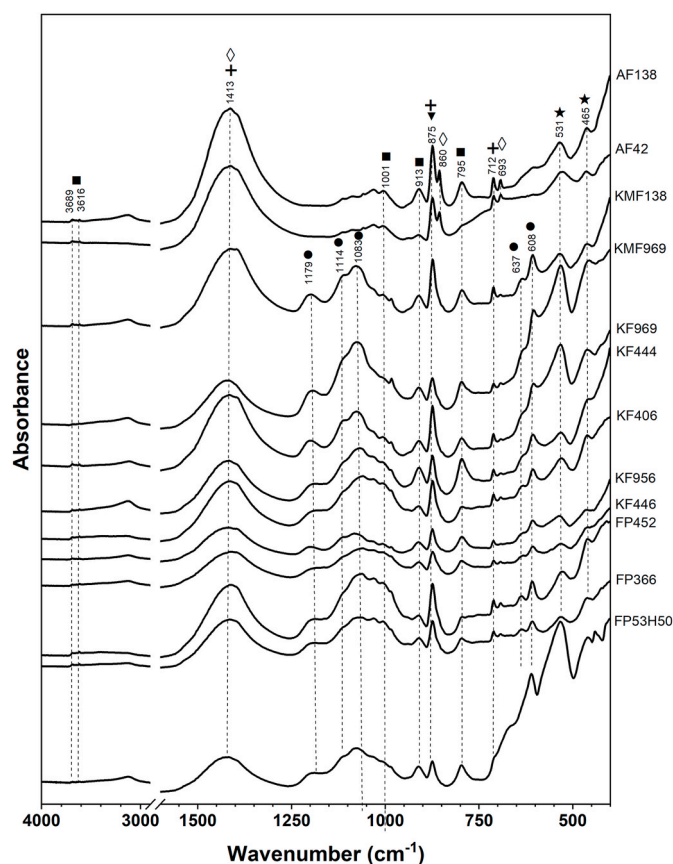


Fig. 4. ATR-FTIR spectra of the twelve samples under investigation. Diagnostic bands of calcite (+), kaolinite (■), barite (●), hematite (★), witherite (◇) and goethite (▼) are evidenced.

samples are characterized by the signals of witherite (BaCO_3) instead (ν_3 (asymmetric stretch) at 1445 cm^{-1} , ν_2 (out-of-plane bending) at 860 cm^{-1} and ν_4 (in-plane bending) band at 693 cm^{-1}) [27]. No organic substances were identified in the pigment admixtures by infrared or, if present, they fall under the detection limit.

3.2.3. Raman spectroscopy

Raman analysis confirmed the results obtained by ATR-FTIR, identifying calcite (1088 cm^{-1} (ν_1) [28–30]), barite (988 cm^{-1} (ν_1) [4,29,31]) and hematite (220 cm^{-1} (A_{1g}), 286 cm^{-1} (E_g) and 1320 cm^{-1} (two-magnon scattering) [28,32]) in all samples (Fig. 5a,b,c,d,e). In addition, it permitted the identification of goethite (main peak at 387 cm^{-1} (B_{3g}) [32,33]) and witherite (134 , 151 and 1052 cm^{-1} (ν_1) [29,34]. New compounds were also identified, such as titanium dioxide in the rutile form (447 cm^{-1} (E_g) and 609 cm^{-1} (A_{1g}) [35]), detected in all samples besides KMF138. Eskolaite (552 cm^{-1} (A_{1g}) [36,37]) was identified in sample FP53H50 (Fig. 5d), which explains the presence of Cr detected by XRF.

When the Raman laser was directed onto the different colored aggregates in sample KMF969, dissimilar Raman spectra were collected and selective detection of witherite and fluorite (CaF_2) was obtained (Fig. 5e and f). Fluorite shows a strong fluorescence band in the $1000\text{--}2500\text{ cm}^{-1}$ region (1113 , 1150 , 1224 , 1316 , 1447 , and 1876 cm^{-1}) [38]) in all samples excluding FP53H50 (Fig. 5d). Only when fluorite was selectively detected in sample KMF969, the signal at 319 cm^{-1} (T_{2g}), which is characteristic for all fluorite-based structures, was observed [38]. Identification using Raman spectroscopy showed variable alignment with reference spectra, matching RRUFF R050045 and RRUFF R050046 [39] (Fig. 5e). The two reference spectra exhibit significantly different fluorescence bands in the $1000\text{--}2500\text{ cm}^{-1}$ region. Such differences may result from variations in rare earth elements (REE)-related

fluorescence, suggesting that those bands are sensitive to the trace-elemental composition of fluorite and may, in turn, provide insights into its provenance.

3.2.4. XRD and semi-quantitative identification by rietveld refinement

XRD analysis supported the identification of eleven different phases among the investigated samples, which can be divided into coloring agents (pigments) and fillers/additives depending on their color and refractive index [41]. No organic materials were observed. The detected phases are:

Pigments: goethite ($\alpha\text{-FeOOH}$, yellow), hematite ($\alpha\text{-Fe}_2\text{O}_3$, red), eskolaite (Cr_2O_3 , green), rutile (TiO_2 , white), and zincite (ZnO , white);

Fillers or additives: calcite (CaCO_3), fluorite (CaF_2), witherite (BaCO_3), barite (BaSO_4), quartz (SiO_2), and kaolinite ($\text{Al}_2\text{Si}_2\text{O}_5(\text{OH})_4$).

Despite of the coexistence of a high number of phases (up to eleven in a single sample), all Rietveld refinements in this study reached convergence, showing relatively good agreement between the observed and the calculated XRD patterns (Supplementary: Table A.12 and Figure A.3). Only one weak peak at $2\theta = 14.12^\circ$ remained unassigned. Fig. 6 shows two representative XRD patterns, one without and one with this additional signal. Specifically, in the *Anstrich Farben* samples all phases were identified (Fig. 6a), whereas the remaining XRD patterns exhibit the additional peak, corresponding to $\sim 2\text{ wt\%}$ of the total composition (Fig. 6b). One could infer that this peak may belong to a Na–Al silicate (albite-type solid solution compound). Fig. 7 presents the phase compositions for each sample, showing the relative quantities (% wt) of each constituent determined through Rietveld refinement.

Based on the quantitative analysis (Fig. 7), fillers were found to predominate in the admixtures, while pigments generally account for less than half of the total composition. The only exception is sample FP53H50, which contains a high pigment content of nearly 50 wt%. All samples investigated in this study contain relatively high percentage of calcite 28(3) wt.% as the main filler component, followed by fluorite 22 (4) wt%. On the other hand, kaolinite differs from sample to sample. The higher amount of kaolinite 20(2) wt.% was determined in the category *Keim Mineral Farben* whereas the other categories exhibit 13(5) wt%. The amount of quartz does not show obvious differences among categories. Three categories KF, KMF, and FP show 9(2) wt.% barite with a minor quantity of witherite less than 5(1) wt%. In comparison, the category AF shows higher content of witherite 12(1) wt.% as an alternative filler.

4. Samples comparison and analytical methods evaluation

The twelve samples share the same composition in terms of pigments (goethite, hematite, rutile, and zincite) and fillers (calcite, fluorite, kaolinite, quartz, barite, rutile, and witherite), with two exceptions: i) eskolaite, present exclusively in KF956, KF969 and FP53H50, and ii) barite which lacks in AF42 (Fig. 7). Hue variations are mainly achieved by varying the amounts of hematite, goethite, and eskolaite (Fig. 7). A good linear correlation between Fe counts (XRF) and the total concentration of Fe-based phases (hematite + goethite) determined by Rietveld refinement of XRD data ($R^2 = 0.8735$) is observed (Fig. 8). This trend aligns with the color shift from light yellow (AF42, FP452, FP366) to orange (KF406, KMF138, KF446, AF138) and dark brown (KMF969, KF969, FP53H50).

As summarized in Table 2, XRD successfully identified all phases, with quartz being the only phase detected exclusively by this method. XRF reliably detected Zn even at 1 %, suggesting that on-site detection would not be problematic. Eskolaite was identified by XRD in four samples, but Cr was detected by XRF only in FP53H50 (19 % eskolaite), indicating that Cr levels in KF956, KF969, and KMF969 (1.3–3.9 % eskolaite) were below the XRF detection limit.

In situ Raman spectroscopy proved to be well suited for identifying fluorite and titanium dioxide (rutile). In contrast, Ti detection by XRF is hindered due to the overlap of Ti K lines with the Ba K lines from the

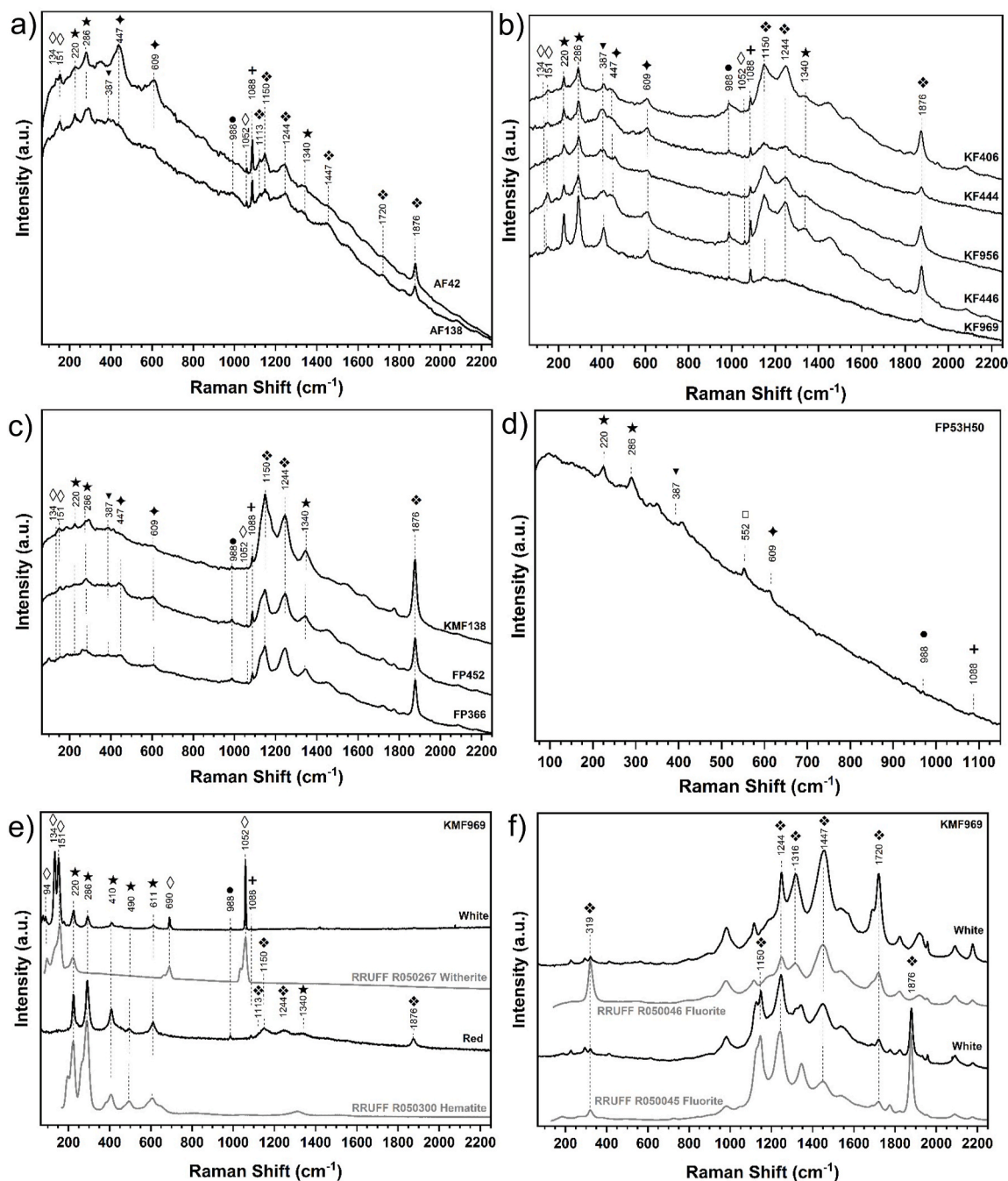


Fig. 5. Raman spectra of the twelve samples under investigation; a) AF42, AF138, b) KF406, KF444, KF956, KF446, KF969, c) KMF138, FP452, FP366, d) FP53H50, e) & f) KMF969 samples. When different colored aggregates were observed, Raman spectra representative of each aggregate are displayed and the color is reported. Diagnostic bands of calcite (+), barite (●), hematite (★), goethite (▼), rutile (◆), witherite (◇), eskolaite (□) and fluorite (♦) are evidenced. The reference Raman spectra from the RRUFF database are displayed in gray for comparison. (For interpretation of the references to color in this figure legend, the reader is referred to the Web version of this article.)

barite and witherite present in high amounts.

Natural fluorite is relevant for distinguishing Keimfarben products [7]. The present study demonstrated that its characteristic fluorescence bands can be excited exclusively with a 785 nm laser in Raman spectroscopy, but not with other excitation wavelengths such as 532 nm [38]. Given the relatively high concentrations of fluorite in the samples and the efficient detection of the fluorescence bands, portable Raman instruments with a 785 nm laser can provide an efficient means of detecting this component in situ [34]. Variations in rare-earth element (REE)-related fluorescence bands may further offer the possibility of

provenance studies, which can help determine the geological sources used [38,40]. However, Raman results can also be influenced by admixture heterogeneity, as reflected in the inconsistent detection of secondary phases such as witherite and goethite across the samples (Table 2).

ATR-FTIR was the only method besides XRD able to identify kaolinite. The application on site of FTIR will imply the use of a reflectance module. Studies showed that, also in reflectance, the kaolinite characteristics bands at 3689 and 3616 cm^{-1} are very easy to detect and no distortion or overlapping with other bands should be

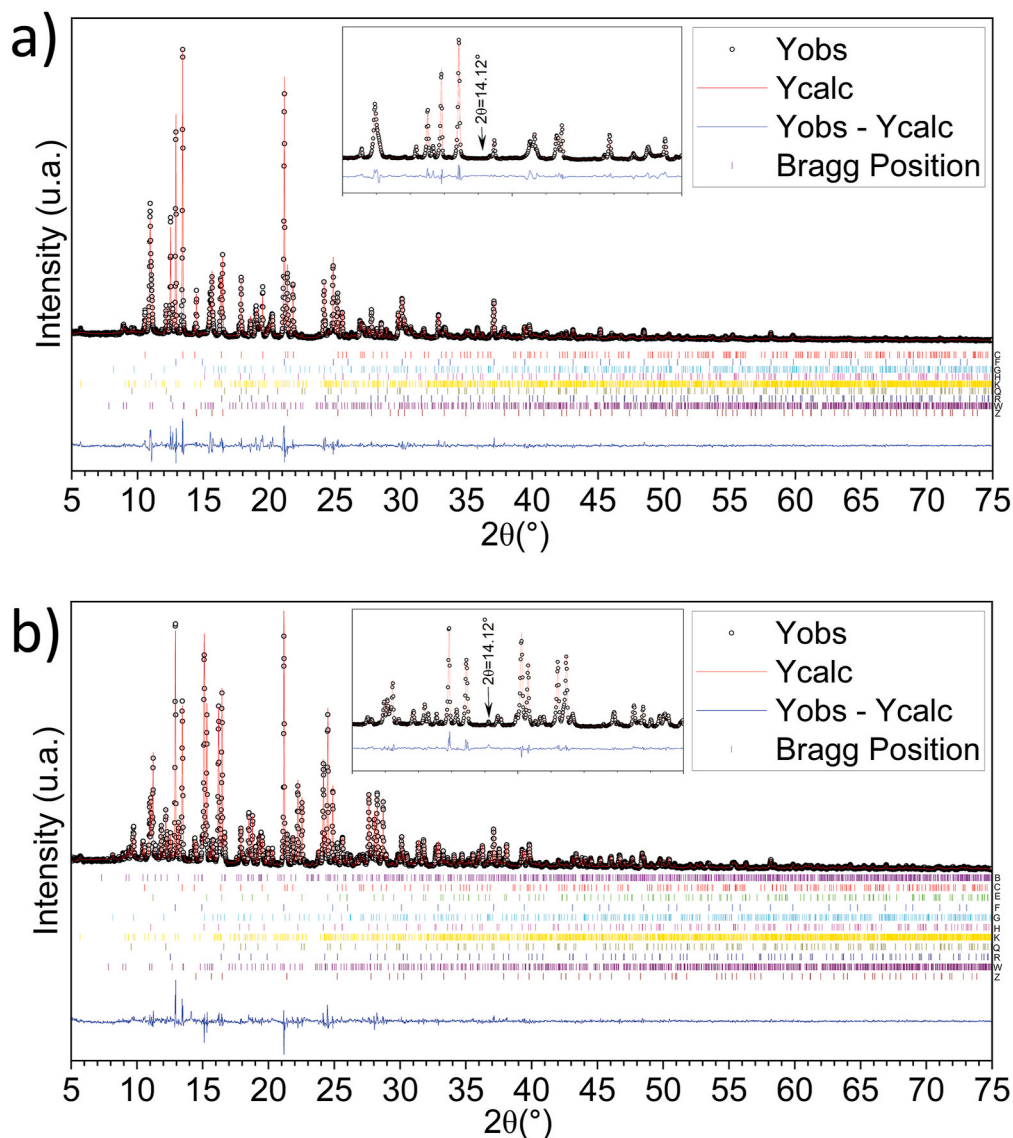


Fig. 6. Phase compositions determined through Rietveld refinement for each sample showing the relative quantities of each constituent. The legend grid uses filled colours to represent colorants, while patterns indicate fillers or additives. (For interpretation of the references to color in this figure legend, the reader is referred to the Web version of this article.)

expected [42].

5. Discussion

Understanding the composition and proportions of the studied pigment admixtures is essential for.

- i) Possible correlation of the composition of specific products with their use for a particular painting technique (A, B, C);
- ii) Understanding the paint system, meaning the role of the ingredients in the formation of the paint coating;
- iii) Tracking formulation changes over time of Keim Farben, as well as the dating of paint layers.

Since only inorganic compounds were identified and the products consist of pigment-filler admixtures, the twelve samples under investigation can be inferred to have been intended for use in *two-component* silicate paint systems. According to the definition in DIN 18,363, this limits their application to *Reinsilikatfarben* (“pure silicate paint systems”) [43].

Optical observations indicate that sample FP53H50, characterized by relatively fine grains under microscopy and a high pigment-to-binder ratio, would be suitable for application using either the A- or B-technique. However, to achieve a more robust differentiation among product categories and establish clearer associations with the A, B, or C application techniques, a larger dataset is required.

The role of individual components (i.e. pigments and fillers) and their proportion within the broader paint system can be contextualized based on historical literature and current research. It is important to emphasize that historical sources generally do not clearly differentiate between pigments and fillers, particularly when describing white compounds. The focus is mostly concentrated on the understanding of their reactivity with the water glass binder.

Understanding the interactions between pigments, fillers, and the silicate binder is central to assessing the curing behavior and long-term stability of silicate-based paints.

Among the factors that are known to improve the setting and stability of the coating (e.g., lowering the pH, loss of water), there are also the so-called “*koagulierender Substanzen*”. In the context of silicate paint coatings, a *coagulating* component typically refers to a material—often a

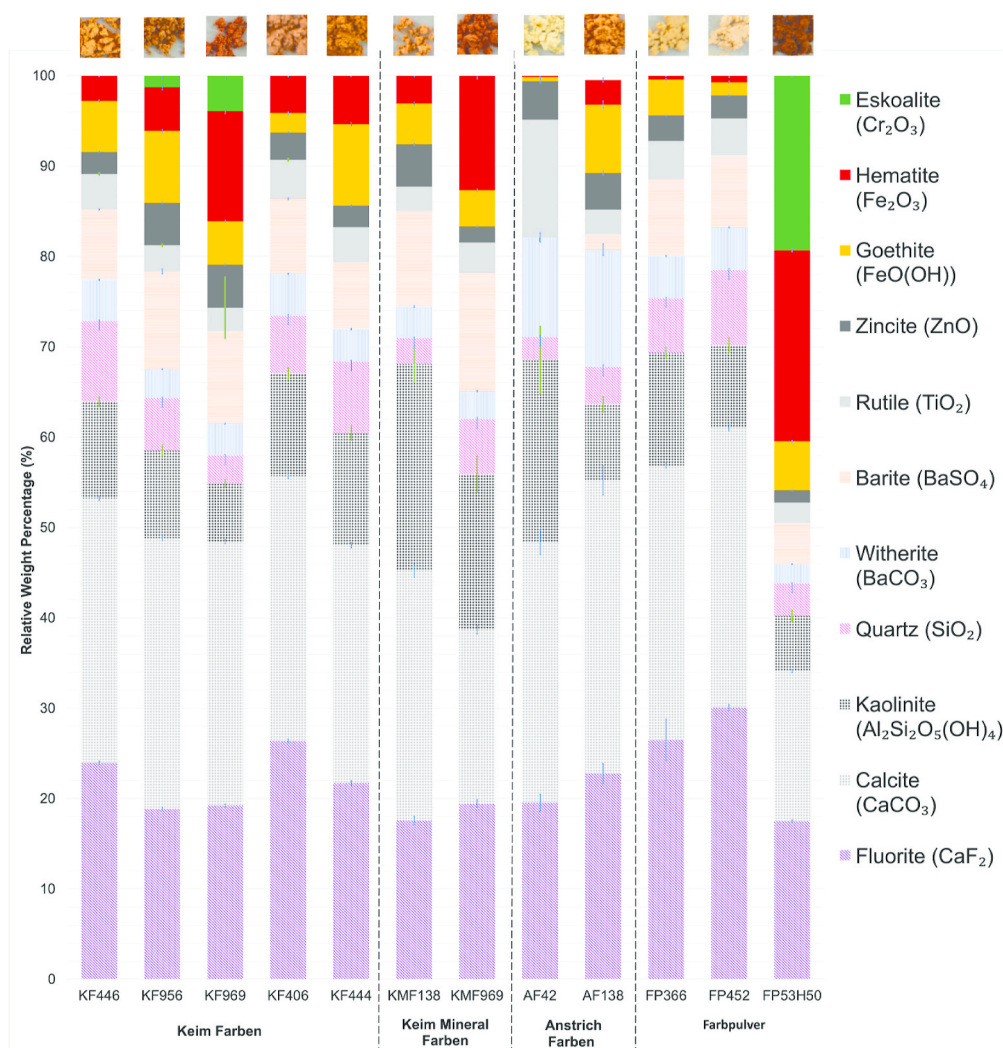


Fig. 7. Graphical representation of results from Rietveld analysis with XRD data observed (circles in black), calculated XRD pattern (in red line) is contributed to the respective relative amount ratio of phase presence in the sample, as indicated with bragg position (in vertical stroke). The agreement factors between the observed and calculated data reflect the difference profile (in blue) at the bottom. The phases identified within samples includes barite (B), calcite (C), eskolaite (E), fluorite (F), goethite (G), hematite (H), kaolinite (K), quartz (Q), rutile (R), witherite (W), and zincite (Z). (a) is the results from sample AF42, with $R_{wp} = 10\%$ and $GoF = 1.7$. (b) is the results from sample FP53H50, with $R_{wp} = 8.6\%$ and $GOF = 1.4$. (For interpretation of the references to color in this figure legend, the reader is referred to the Web version of this article.)

finely dispersed pigment, filler, or other additive—that interacts with the silicate binder (commonly potassium water glass) in such a way that it promotes the formation of a stable, solid network [1]. As Osswald describes [6], the gel formation in silicate paints is primarily initiated by multivalent cations, which bind to oxygen groups on the silicate particles. This interaction creates positively charged sites that enable electrostatic attraction between particles, promoting condensation via their hydroxyl groups and ultimately contributing to the formation of a coherent silicate network. Therefore, the presence and nature of pigments and fillers can significantly influence the kinetics and structure of the gelation process [6].

In general, all pigments used in silicate paint should present high stability in alkaline conditions. However, as Max Doerner wrote, the palette of pigments used for this technique is even more limited than the one used in fresco paintings [5]. Since the alkali condition in water glass is comparable to that in quick lime, Doerner probably refers to the reactivity with the binder and their role in the creation of the coating, and/or to their purity. Metal oxide, -oxidehydrate, and silicate are in fact reacting at the particle interfaces with the binder forming silicate bonding (e.g., Zn_2SiO_4 ; Fe_2SiO_4). Schönburg was able by means of

Scanning Electron Microscopy (SEM) to investigate the formation of zinc silicate crystals around the particle demonstrating its important role in the formation of a stable paint system [8]. Already in 1881 (Patent D.R. P. 19210), Keim specifically mentioned that zincite as well as calcite, quartz, aluminum oxide hydrate (kaolinite), and magnesia (MgO) facilitate bonding with the binder.

Alp et al. [7] observed that zinc white is the component that distinguished Keim products from other companies producing silicate paints between 1930 and 1940s. In 1893, Keim patented a new formulation in which barite, along with aluminosilicate, was included in the admixture to enhance the binding power (Patent D.R.P. 82047). Keim's approach to evaluating the new improvement was empirical; therefore, the role of barite remains unclear and should be further investigated.

Doerner in the 1930s listed among the components of Keimfarben calcite, zincite, quartz, and magnesia [5]. Wehlte listed, along with the mentioned components, also barite, aluminum silicate (kaolinite) and witherite [44]. Interestingly, no Mg-based phases were identified in the samples analyzed. Again, the detection of such phases could be attributed to earlier products. However, Alp et al. also did not detect these compounds in products between 1930 and the 1940s [7].

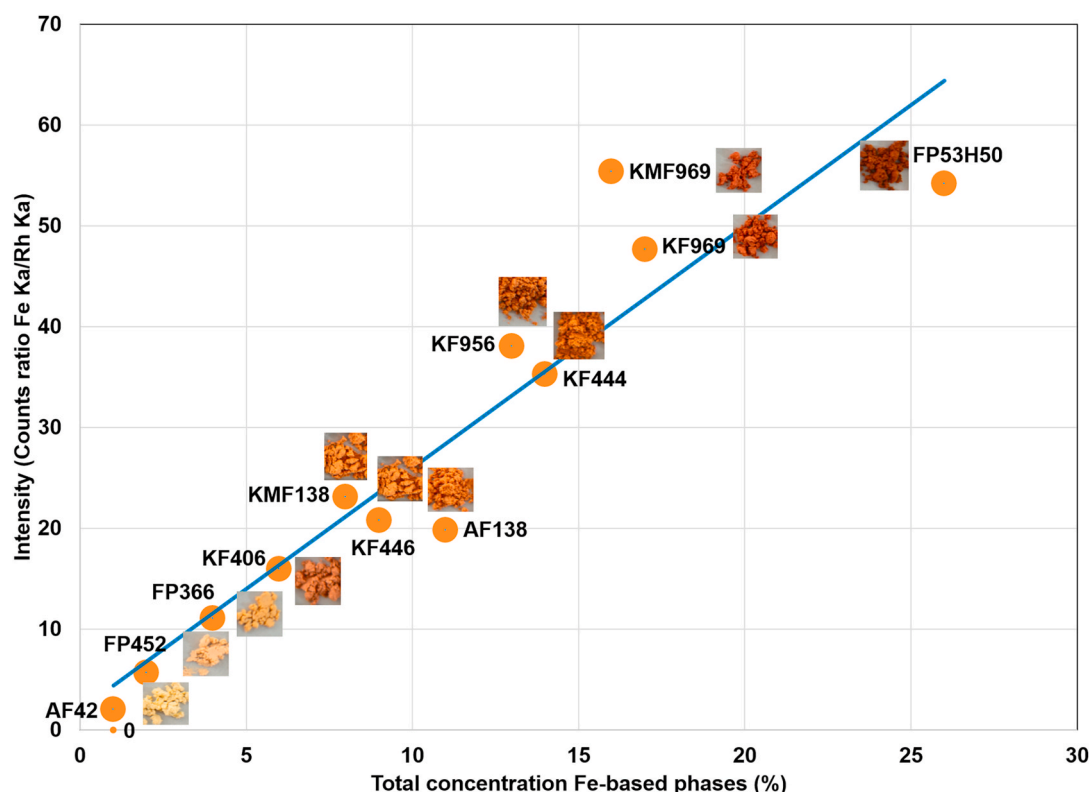


Fig. 8. Correlation between Fe counts (Fe K_{α} /Rh K_{α} ratio) and the total concentration of Fe-based phases (hematite + goethite) determined by Rietveld refinement of XRD data. The colour progression from light yellow to orange and dark brown aligns with increasing Fe content, with slight deviations in the darkest samples attributed to Eskolaite-induced hue modulation. (For interpretation of the references to color in this figure legend, the reader is referred to the Web version of this article.)

Table 2

Summary of the phases identified in each sample and the analytical methods that detected them (a-XRF; b-XRD; c-ATR-FTIR; d-Raman).

Samples	Fluorite (CaF_2)	Calcite (CaCO_3)	Kaolinite ($\text{Al}_2\text{Si}_2\text{O}_5(\text{OH})_4$)	Quartz (SiO_2)	Witherite (BaCO_3)	Barite (BaSO_4)	Rutile (TiO_2)	Zincite (ZnO)	Goethite ($\text{FeO}(\text{OH})$)	Hematite (Fe_2O_3)	Eskolaite (Cr_2O_3)
AF_42	a b d	a b c d	b c	b	a b c d	Not detected	a(?) b d	a b	a b c	a b c d	–
AF_138	a b d	a b c d	b c	b	a b c d	a b d	a(?) b d	a b	a b c d	a b c d	–
KF_406	a b d	a b c d	b c	b	a b	a b c d	a(?) b d	a b	a b c d	a b c d	–
KF_444	a b d	a b c d	b c	b	a b	a b c d	a(?) b d	a b	a b d	a b c d	–
KF_446	a b d	a b c d	b c	b	a b d	a b c d	a(?) b d	a b	a b d	a b c d	–
KF_956	a b d	a b c d	b c	b	a b	a b c d	a(?) b d	a b	a b d	a b c d	b
KF_969	a b d	a b c d	b c	b	a b	a b c d	a(?) b d	a b	a b c d	a b c d	b
KMF_138	a b d	a b c d	b c	b	a b d	a b c d	a(?) b	a b	a b c d	a b c d	–
KMF_969	a b d	a b c d	b c	b	a b d	a b c d	a(?) b d	a b	a b	a b c d	b
FP_366	a b d	a b c d	b c	b	a b d	a b c d	a(?) b d	a b	a b c d	a b c d	–
FP_452	a b d	a b c d	b c	b	a b d	a b c d	a(?) b d	a b	a b c d	a b c d	–
FP_53H50	a b	a b c d	b c	b	a b	a b c d	a(?) b d	a b	a b d	a b c d	a b d

(?) Indicates the detection of the $\text{Ti } K_{\alpha,\beta}$ lines (4.51 and 4.93 keV), with uncertain attribution due to overlap with the first two barite lines.

Understanding the evolution of Keim products' formulation from the first patent to the present is beyond the scope of this study. However, contextualizing the findings with the literature, the components identified in the admixture are mostly described as traditional pigments and fillers used in mineral paint systems. With the exception of rutile, witherite and fluorite, all the compounds were already mentioned by A. Keim in his first patent [45].

Hematite, goethite and eskolaite are the colored pigments identified in the samples. In 1881, Keim mentions that iron oxides are very stable and he remarks their usability in all painting techniques [4]. Ochre pigments in general are extremely stable, non-fading with a strong tinting strength. They are used in the construction, coating and paint industries and are among the few pigments approved by the American Society for Testing and Materials (ASTM) [46].

Keim use the terms "*erdfarben und eisenoxide*" (earth colours and iron oxide) referring to the natural ochres. Specifically, he properly described the red colored compounds as "*ironoxid*" (iron oxide), which means hematite, and the yellow-colored compounds as "*ironoxidhydrat*" (iron oxide hydrate), indicating goethite. He refers to darker hues as associated with brown ochre/burnt sienna [4]. The use of natural ochre seems to be common for mineral paint [5,8,44]. However, typical phases that can indicate the presence of natural ochre along with hematite and goethite, such as related minerals as dolomite $\text{CaMg}(\text{CO}_3)_2$, illite $(\text{K}, \text{H}_3\text{O})(\text{Al})_2(\text{Si}, \text{Al})_4\text{O}_{10}[(\text{OH})_2, \text{H}_2\text{O}]$, as well as limonite in yellow shades and/or MnO_2 for the brown/burned variation were not identified in the studied samples [21,47]. The CEO of the company, Thomas Klug, uses the term "synthetic" in general to describe the pigments used for the admixture, confirming our findings [43]. Unfortunately, no systematic

studies have been published on the analysis of dark brown shades of Keim products produced up to the 1960s. In theory, the presence of natural ochre pigments may indicate early products; thus, their detection within a paint stratigraphy could point to chronologically older paint layers. Instead of brown pigments, the green eskolaite (chromium oxide) was used to obtain darker/brownish tones in samples KF956, KF969 and FP53H50.

Indeed, pigments as red, brown and yellow ochre, whose main components are iron oxides, as well as both chromium hydroxide green and chromium oxide, were already part of the so call “*Normalfarben-Skala*” (Normal color scaler) [48], a list of high quality pigments suggested by Keim and the “*Deutsche Gesellschaft zur Beförderung rationeller Malverfahren*” (DGzBrM; Engl. Society for the Promotion of Rational Painting Techniques). This commission, founded by A. W. Keim in Munich in 1886, was meant to promote quality in paint products at the beginning of the industrial revolution [49]. By the 1930s, synthetic iron oxides had largely replaced natural ochres and iron oxide pigments in many applications, though natural pigments remained in use in specific traditional or artistic contexts [41].

Rutile is recognized as the most stable crystalline phase of titanium dioxide (TiO_2), a very common white pigment used in a variety of applications. The production of titanium white in its pure rutile form, as identified in the samples analyzed in this study, only became industrially viable following the introduction of the chloride process in 1958 [50–52]. This technological advancement marked a significant shift in pigment manufacturing. Notably, titanium white was not detected—not even in the anatase form—in specimens dated between 1920 and 1930, as reported by Alp et al. The consistent presence of rutile in the samples studied, therefore, provides a terminus post quem, situating their production no earlier than the late 1950s.

Witherite (barium carbonate, BaCO_3) was first classified as Pigment White 10 (C.I. 77099) in the second edition of the *Colour Index*, published in 1956 [53]. Its use in Keim formulations is first explicitly mentioned by Wehlte in 1967 [54], where it is described as a minor extender component in combination with other pigments. The synthetic form of barium carbonate had previously been defined in British Standard BS 1795:1952 [49]. In addition to its application in paint, it was also used in rat poison, highlighting its acute toxicity—a property confirmed by toxicological studies such as the one by Diechmann and Gerarde published already in 1969 [55,56].

According to an interview with the former head chemist of Keimfarben, the use of barium carbonate in their formulations was either discontinued or drastically reduced starting in 1981, in response to increasingly stringent regulatory restrictions due to its toxicity (Interview Chemist Keim). While it cannot be fully excluded that witherite occurs as a natural impurity—potentially as a secondary mineral associated with natural sources of calcite, barite, or fluorite—the relatively high and consistent concentrations observed in the studied samples (ranging from 5 % to 13 %) argue against this hypothesis. Instead, the most feasible use of synthetic barium carbonate as a functional additive during the production phase, can be postulated [50]. This contextual information suggests that the presence of witherite in the analyzed samples can be considered consistent with a production date between 1952 and the early 1980s. Interestingly, the Industrierwerke Lohwald plant ceased its operations precisely in 1978.

Fluorite was already included in the second patent (*D.R.P. 21874*) as a component of the pigment and filler admixtures. The third patent *D.R.P. 38415 (1883)* outlines a simplified method of paint production, wherein pigments are combined with a substrate composed of fluorite (CaF_2), freshly precipitated soluble silica ($\text{SiO}_2 \cdot x\text{H}_2\text{O}$), calcium carbonate (CaCO_3), magnesium carbonate (MgCO_3), alumina (Al_2O_3), and calcium silicate ($\text{Ca} \cdot y\text{SiO}_2 \cdot z\text{H}_2\text{O}$). This mixture was then blended with a fixative to produce a ready-to-use paint [6]. Alp et al. showed that fluorite (CaF_2) is not exclusive to Keim colours, as it also appears in other brands from the 1920s–1930s. However, it remained a consistent component in Keim formulations as natural phase [7].

In the present study, fluorite was likewise identified in the analyzed Keim samples as a natural compound. Interestingly, two distinct Raman spectra were obtained, both matching reference data from the RRUFF database corresponding to fluorite of Chinese origin (Hunan Province). According to literature (available only in Chinese), large-scale fluorite ore exploitation in Europe began in 1946; however, resource shortages later led to the import of Chinese material. Specifically, mining activities in Hunan Province commenced only in 1960, driven by increasing global industrial demand [57]. Comparative analyses of German fluorite (results not shown) revealed very similar spectra, preventing firm provenance attribution. However, given that Chinese fluorite was only commercially exploited from the 1960s onwards, its potential presence would be relevant to clarify chronological aspects of the Keim products. Further determination of rare earth elements (REE) will possibly help unlock the provenance.

6. Conclusions

This study provides the first comprehensive material characterization and quantitative phase analysis of a selection of yellow-to brownish-toned historical *Keim'sche Mineralfarben* pigment admixtures, using a multi-analytical approach that combines non-invasive and laboratory-based techniques, including the first application of Rietveld refinement to this type of material.

The results show that all investigated admixtures are composed of a consistent base mixture of calcite, fluorite, kaolinite, quartz, barite, rutile, and witherite, combined with variable amounts of hematite, goethite, and eskolaite (only in KF956, KF969, and KMF969) to modulate the color. Barite was not detected only in sample AF42.

The detection and/or absence of valuable provides chronological information narrowing the date of the products to a timeframe between the 1958 and 1980s.

- Rutile (TiO_2), indicates production after the late 1950s, following the industrial introduction of the chloride process.
- Witherite (BaCO_3), detected in relatively high and consistent amounts, points to a production window between the 1950s and early 1980s, before its use was discontinued for safety reasons.
- Eskolaite (Cr_2O_3), found in darker hues, together with the absence of e.g. manganese dioxide (MnO_2), indicates the use of chromium-based pigments to produce brown tones, replacing natural ochres.

The study also demonstrates the diagnostic potential of portable methods.

- XRF proved sensitive for detecting zinc and other major elements such as iron. Zinc in particular may be key to distinguishing Keim admixtures in silicate coatings from those of other companies.
- In situ Raman spectroscopy reliably identified witherite, barite, rutile and fluorite. The 785 nm laser proved to be effective for fluorite identification.
- ATR-FTIR showed to be important for Kaolinite detection. The in situ recording of FTIR spectra would be possible using a reflectance module.

The availability of original Keimfarben product packaging provides a valuable context for understanding their history and attributing samples to specific production periods. In built heritage, however, such contextual evidence is rarely available, particularly for materials already applied or originating from undocumented conservation interventions. This makes reliable analytical approaches for compositional analysis essential. The present study shows that the identification of specific compounds and mineral phases can serve as diagnostic markers, supplying valuable terminus ante quem and terminus post quem information for chronological attribution. When detected in situ, these markers offer a promising tool for distinguishing historical paint layers from later

interventions. Overall, the results demonstrate that historical Keimfarben pigment admixtures can be differentiated and potentially dated through their mineralogical composition, providing new opportunities for stratigraphic analysis and for supporting conservation strategies on architectural surfaces.

CRedit authorship contribution statement

Yee Wu: Writing – review & editing, Writing – original draft, Visualization, Investigation, Formal analysis. **Eva Mariasole Angelin:** Writing – review & editing, Writing – original draft, Visualization, Validation, Supervision, Investigation, Formal analysis. **Thomas Danzl:** Writing – review & editing, Supervision, Resources, Funding acquisition. **SoHyun Park:** Writing – review & editing, Validation, Supervision, Resources, Methodology. **Clarimma Sessa:** Writing – review & editing, Writing – original draft, Visualization, Validation, Supervision, Project administration, Methodology, Investigation, Funding acquisition, Formal analysis, Data curation, Conceptualization.

Declaration of generative AI and AI-assisted technologies in the writing process

While preparing this work, the author used ChatGPT 4.0 to improve solely the readability and language of the manuscript. After using this service, the authors reviewed and edited the content as needed and take full responsibility for the content of the published article.

Funding

The present work was carried out with the support of the "insituTUMlab. Analytical infrastructure for non-destructive in-situ studies of Cultural Heritage", funded by the Deutsche Forschungsgemeinschaft (DFG, German Research Foundation) – Project No. 492717225.

Declaration of competing interest

The authors declare that they have no known competing financial interests or personal relationships that could have appeared to influence the work reported in this paper.

Acknowledgments

The authors would like to thank Susanne Oberrauch for donating the valuable historical collection for research purposes, recognizing the importance of historical material references. We are grateful to Thomas Klug (CEO of Keimfarben), current Keim chemist Florian Zimmerly, and former laboratory manager Franz Heiberger for sharing insights on Keim product formulations. We also thank Kathrin Kinseher for facilitating contacts and providing helpful background information. Finally, we wish to acknowledge the colleagues Zeynep Alp, Jana Hainbach and Christoph Herm for their extensive research on early Keim products, which greatly supported the interpretation of our findings.

Appendix A. Supplementary data

Supplementary data to this article can be found online at <https://doi.org/10.1016/j.dyepig.2025.113285>.

Data availability

Data will be made available on request.

References

- [1] Mineralfarben: Beiträge zur Geschichte und Restaurierung von Fassadenmalereien und Anstrichen; [Weiterbildungstagung des Instituts für Denkmalpflege an der ETH

- Zürich „Erfahrungen mit der Restaurierung von Mineralfarbenmalereien“, 20. - 22. März 1997. Zürich: vdf Hochsch.-Verl. an der ETH; 1998.
- [2] Kinseher K. „Womit sollen wir malen?“: farben-streit und maltechnische Forschung in München; ein Beitrag zum Wirken von Adolf Wilhelm Keim. Siegl, München: Zugl. geringfügig überarb. Fassung von: München, Univ., Diss; 2013. 2014.
- [3] Schönburg K. Mineralfarbentechnik am bauwerk: Vorteile, anwendung, ausführung, beurteilung. second. Berlin, Wien, Zürich: überarb. und erw. Aufl., Beuth; 2013.
- [4] Keim AW. Die Mineral-Malerei: neues Verfahren zur Herstellung witterungsbeständiger Wandgemälde; technisch-wissenschaftliche Anleitung, Nachdr. der Ausg. von eighteenthfirst. Stuttgart: Enke; 1995.
- [5] Doerner M. Malmaterial und seine Verwendung im Bilde, eighteenth. Stuttgart: Aufl., Enke; 1994.
- [6] Osswald J. Die Struktur und Reaktionen des Kiesel säuregels in den Silikatfarben der Keim'schen Mineralmalerei. München: Dissertation; 1996.
- [7] Alp Z, Hainbach J, Herm C, Danzl T. 'Keim'sche Mineralfarben' marker: is it a myth? A comprehensive analytical study of its detection methods and true nature. Constr Build Mater 2025;475:141051. <https://doi.org/10.1016/j.conbuildmat.2025.141051>.
- [8] Schönburg K. Historische Beschichtungstechniken: erhalten, Bewerten und Anwenden. thirdrd ed. Beuth Verlag; 2011. Erscheinungsort nicht ermittelbar.
- [9] Dobras W. Zur Bemalung des Lindauer Alten Rathauses. Schriften des Vereins für Geschichte des Bodensees und seiner Umgebung 1975;93:115–8.
- [10] Oberrauch S. Use of Keimfarben in lindau. 2024. Lindau.
- [11] Gettwert G, Rieber W, Bonarius J. One-component silicate binder systems for coatings. Surf Coating Int 1998;81:596–603. <https://doi.org/10.1007/BF02693054>.
- [12] Elsner H. A-, B- und C-Technik anhand von Beispielen. In: Mineralfarben: Beiträge zur Geschichte und Restaurierung von Fassadenmalereien und Anstrichen; [Weiterbildungstagung des Instituts für Denkmalpflege an der ETH Zürich „Erfahrungen mit der Restaurierung von Mineralfarbenmalereien“, 20. - 22. März 1997, vdf Hochsch.-Verl. an der. Zürich: ETH; 1998. p. 107–10.
- [13] Schönburg K, editor. Historische Beschichtungstechniken: erhalten, Bewerten und Anwenden. fourth ed. Berlin: DIN Media GmbH; 2024.
- [14] Baugestaltungssatzung der Stadt Lindau, Bodensee., § 5 Fassadenmalerei, Fassadenfarben, Fassadengliederung. 2011.
- [15] Dr H. Putz & Dr K. Brandenburg GbR, Match! - phase analysis using powder diffraction: crystal impact, Kreuzherrenstr. 102, 53227 Bonn, Germany..
- [16] Vaitkus A, Merkys A, Sander T, Quirós M, Thiessen PA, Bolton EE, Gražulis S. A workflow for deriving chemical entities from crystallographic data and its application to the Crystallography Open Database. J Cheminform 2023;15:123. <https://doi.org/10.1186/s13321-023-00780-2>.
- [17] Gražulis S, Chateigner D, Downs RT, Yokochi AFT, Quirós M, Lutterotti L, Manakova E, Butkus J, Moeck P, Le Bail A. Crystallography Open Database - an open-access collection of crystal structures. J Appl Crystallogr 2009;42:726–9. <https://doi.org/10.1107/S0021889009016690>.
- [18] Young RA, editor. The Rietveld method. Oxford: Oxford Univ. Press; 1995.
- [19] Coelho AA. TOPAS and TOPAS-Academic an optimization program integrating computer algebra and crystallographic objects written in C++. J Appl Crystallogr 2018;51:210–8. <https://doi.org/10.1107/S1600576718000183>.
- [20] Zagorac D, Müller H, Ruehl S, Zagorac J, Rehme S. Recent developments in the inorganic Crystal Structure Database: theoretical crystal structure data and related features. J Appl Crystallogr 2019;52:918–25. <https://doi.org/10.1107/S160057671900997X>.
- [21] Genestar C, Pons C. Earth pigments in painting: characterisation and differentiation by means of FTIR spectroscopy and SEM-EDS microanalysis. Anal Bioanal Chem 2005;382:269–74. <https://doi.org/10.1007/s00216-005-3085-8>.
- [22] Dewi R, Agusnar H, Alfian Z. Tamrin, Characterization of technical kaolin using XRF, SEM, XRD, FTIR and its potentials as industrial raw materials. J Phys: Conf Ser 2018;1116:42010. <https://doi.org/10.1088/1742-6596/1116/4/042010>.
- [23] Čiuladienė A, Luckutė A, Kiuberis J, Kareiva A. Investigation of the chemical composition of red pigments and binding media. Chemija 2018;29. <https://doi.org/10.6001/chemija.v29i4.3840>.
- [24] Cornell RM, Schwertmann U. The Iron oxides. Wiley; 2003.
- [25] Prasad P, Shiva Prasad K, Krishna Chaitanya V, Babu E, Sreedhar B, Ramana Murthy S. In situ FTIR study on the dehydration of natural goethite. J Asian Earth Sci 2006;27:503–11. <https://doi.org/10.1016/j.jseas.2005.05.005>.
- [26] Adler HH, Kerr PF. Variations in infrared spectra, molecular symmetry and site symmetry of sulfate minerals. Am Mineral 1965;50:132–47.
- [27] Huang CK, Kerr PF. Infrared study of the carbonate minerals. Am Mineral 1960;45:311–24.
- [28] Bell IM, Clark RJ, Gibbs PJ. Raman spectroscopic library of natural and synthetic pigments (pre- approximately 1850 AD). Spectrochim Acta Mol Biomol Spectrosc 1997;53A:2159–79. [https://doi.org/10.1016/S1386-1425\(97\)00140-6](https://doi.org/10.1016/S1386-1425(97)00140-6).
- [29] Burzio L, Clark RJ. Library of FT-Raman spectra of pigments, minerals, pigment media and varnishes, and supplement to existing library of Raman spectra of pigments with visible excitation. Spectrochim Acta Mol Biomol Spectrosc 2001;57:1491–521. [https://doi.org/10.1016/S1386-1425\(00\)00495-9](https://doi.org/10.1016/S1386-1425(00)00495-9).
- [30] Gunasekaran S, Anbalagan G, Pandi S. Raman and infrared spectra of carbonates of calcite structure. J Raman Spectroscopy 2006;37:892–9. <https://doi.org/10.1002/jrs.1518>.
- [31] Jehlička J, Vítek P, Edwards H, Hargreaves MD, Čapoun T. Fast detection of sulphate minerals (gypsum, anglesite, baryte) by a portable Raman spectrometer. J Raman Spectroscopy 2009;40:1082–6. <https://doi.org/10.1002/jrs.2246>.

- [32] de Faria DLA, Venâncio Silva S, de Oliveira MT. Raman microspectroscopy of some iron oxides and oxyhydroxides. *J Raman Spectroscopy* 1997;28:873–8. [https://doi.org/10.1002/\(SICI\)1097-4555\(199711\)28:11<873::AID-JRS177>3.0.CO;2-B](https://doi.org/10.1002/(SICI)1097-4555(199711)28:11<873::AID-JRS177>3.0.CO;2-B).
- [33] Abrashev MV, Ivanov VG, Stefanov BS, Todorov ND, Rosell J, Skumryev V. Raman spectroscopy of α -FeOOH (goethite) near antiferromagnetic to paramagnetic phase transition. *J Appl Phys* 2020;127:205108. <https://doi.org/10.1063/5.0006352>.
- [34] Buzgar N, Apopei AI. The Raman study of certain carbonates. In: *Analele Stiintifice de Universitati A.I. Cuza din Iasi. Sect. 2, Geologie*, vol. 55; 2009. p. 97–112. <https://doi.org/10.13140/2.1.1358.3368>.
- [35] Balachandran U, Eror NG. Raman spectra of titanium dioxide. *J Solid State Chem* 1982;42:276–82. [https://doi.org/10.1016/0022-4596\(82\)90006-8](https://doi.org/10.1016/0022-4596(82)90006-8).
- [36] Bhardwaj P, Singh J, Kumar R, Kumar D, Verma V, Kumar R. Oxygen defects induced tailored optical and magnetic properties of $\text{FeCr}_2\text{-xO}_3$ ($0 \leq x \leq 0.1$) nanoparticles. *Appl Phys A* 2022;128. <https://doi.org/10.1007/s00339-021-05233-x>.
- [37] Brown DA, Cunningham D, Glass WK. The infrared and Raman spectra of chromium (III) oxide. *Spectrochim Acta Mol Spectrosc* 1968;24:965–8. [https://doi.org/10.1016/0584-8539\(68\)80115-1](https://doi.org/10.1016/0584-8539(68)80115-1).
- [38] Čermáková Z, Bezdička P, Némec I, Hradilová J, Šrein V, Blažek J, Hradil D. Naturally irradiated fluorite as a historic violet pigment: raman spectroscopic and x-ray diffraction study. *J Raman Spectroscopy* 2015;46:236–43. <https://doi.org/10.1002/jrs.4627>.
- [39] Lafuente B, Downs RT, Yang H, Stone N. The power of databases: the RRUFF project. In: Armbruster T, Danisi RM, editors. *Highlights in mineralogical crystallography*. Berlin: W. De Gruyter; 2015. p. 1–30.
- [40] Ge X, Guo Q, Wang Q, Li T, Liao L. Mineralogical characteristics and luminescent properties of natural fluorite with three different colors. *Materials* 2022;15. <https://doi.org/10.3390/ma15061983>.
- [41] Hempelmann U, Buxbaum Gunter, Völz Hans G. Introduction. In: Buxbaum G, editor. *Industrial inorganic pigments*, third., completely rev. Weinheim: Wiley-VCH; 2005. p. 1–50.
- [42] Volpi F, Vagnini M, Vivani R, Malagodi M, Fiocco G. Non-invasive identification of red and yellow oxide and sulfide pigments in wall-paintings with portable ER-FTIR spectroscopy. *J Cult Herit* 2023;63:158–68. <https://doi.org/10.1016/j.culher.2023.07.019>.
- [43] Klug T. Silikatfarben. In: Jean G, editor. *Conservation of colour in 20th century architecture*, SUPSI-Nardini Editore; 2013. p. 228–43.
- [44] Wehlte K. *Werkstoffe und Techniken der Malerei: Mit einem Anhang über Farbenlehre*. Ravensburg: fourth. Auflage, Maier-Verlag; 1967.
- [45] A.W. Keim DE000000019210A.
- [46] Elias M, Chartier C, Prévot G, Garay H, Vignaud C. The colour of ochres explained by their composition. *Mater Sci Eng, B* 2006;127:70–80. <https://doi.org/10.1016/j.mseb.2005.09.061>.
- [47] Montagner C, Sanches D, Pedrosa J, Melo MJ, Vilarigues M. Ochres and earths: matrix and chromophores characterization of 19th and 20th century artist materials. *Spectrochim Acta Mol Biomol Spectrosc* 2013;103:409–16. <https://doi.org/10.1016/j.saa.2012.10.064>.
- [48] Eibner A. *Die Normalfarben-Skala: vortrag gehalten in der Adolf Wilhelm Keim-Gesellschaft. Verlag der Technischen Mitteilungen für Malerei München, München*. 1915.
- [49] Sessa C, Steuer C, Quintero Balbas D, Sciutto G, Prati S, Stege H. Analytical studies on commercial artists' colour charts from Das Deutsche Farbenbuch (1925)—identification of synthetic and natural organic colourants by Raman microscopy, surface-enhanced Raman spectroscopy and metal underlayer ATR-FTIR spectroscopy. *Herit Sci* 2022;10. <https://doi.org/10.1186/s40494-022-00740-3>.
- [50] Hering B. *Weisse Farbmittel: ein Nachschlagewerk für Konservatoren, Restauratoren, Studenten, Architekten, Denkmalpfleger, Kunstwissenschaftler, Maler, Sachkundige und Interessierte*. first. Aufl. Fürth: Eigenverl. M. H. B. Hering; 2000.
- [51] Rechmann H. *Titandioxid-Pigmente, hergestellt nach dem Chloridverfahren*. *Deutsche Farben-Zeitschrift* 1978;32:331–8.
- [52] Rechmann H, Klein J. 50 Jahre Titandioxidpigment-industrie: versuch einer Chronologie ihrer wirtschaftlichen Entwicklung. *Farbe Lack* 1967;73:417–24.
- [53] Society of Dyers and Colourists. *Colour Index*. second ed. 1956. supplement, Society of Dyers and Colourists; 1963.
- [54] Wehlte K. *The materials and techniques of painting*. New York: Kremer; 1975.
- [55] Puffer JH. *Toxic minerals*. *Mineral Rec* 1980;11:5–11.
- [56] Deutsche Forschungsgemeinschaft, The MAK collection for occupational health and safety: Begründungen und Methoden documentation and methods, ZB MED - Informationszentrum lebenswissenschaften; Wiley; Wiley-VCH, Köln, Weinheim, Weinheim, früher..
- [57] Wang J, Shang P, Xiong X, Yang H, Tang Y. The classification of fluorite deposits in China. *中国地质英文版* 2014;41:315–25.